Ultrafast Nonlinear Response of Gold Gyroid Three-Dimensional Metamaterials

Petros Farah,[1] Angela Demetriadou,[2] Stefano Salvatore,[1] Silvia Vignolini,[1,6] Morgan Stefik,[3] Ulrich Wiesner,[3] Ortwin Hess,[4] Ullrich Steiner,[1,5] Ventsislav K. Valev,[1] and Jeremy J. Baumberg[1,*]

[1]*Cavendish Laboratory, Department of Physics, University of Cambridge, Cambridge, CB3 0HE, United Kingdom*

[2]*Department of Chemistry, Imperial College London, London, SW7 2AZ, United Kingdom*

[3]*Department of Materials Science and Engineering, Cornell University, Ithaca, New York 14853, USA*

[4]*Blackett Laboratory, Department of Physics, Imperial College London, London SW7 2AZ, United Kingdom*

[5]*Adolphe Merkle Institute, Chemin des Verdiers, CH-1700 Fribourg, Switzerland*

[6]*Department of Chemistry, University of Cambridge, Lensfield Road, Cambridge CB2 1EW, United Kingdom*

(Received 21 April 2014; revised manuscript received 4 September 2014; published 7 October 2014)

We explore the nonlinear optical response of three-dimensional gyroidal metamaterials, which show greater than tenfold enhancements compared to all other metallic nanomaterials as well as bulk gold. A simple analytical model for this metamaterial response shows how the reflectivity spectrum scales with the metal fill fraction and the refractive index of the material that the metallic nanostructure is embedded in. The ultrafast response arising from the interconnected three-dimensional nanostructure can be separated into electronic and lattice contributions with strong spectral dependences on the dielectric filling of the gyroids, which invert the sign of the nonlinear transient reflectivity changes. These metamaterials thus provide a wide variety of tunable nonlinear optical properties, which can be utilized for frequency mixing, optical switching, phase modulators, novel emitters, and enhanced sensing.

DOI: 10.1103/PhysRevApplied.2.044002

I. INTRODUCTION

Optical metamaterials have generated intense interest from the scientific community and captured the imagination by promising a new class of optical media exhibiting extraordinary optical properties [1,2]. The macroscopic optical behavior of these materials arises from the subwavelength structure of their composite materials. Wide design freedom in the metamaterial subunits allows the realization of artificial materials with unique optical properties, such as negative refraction [3] and optical cloaking [4]. However, only in the last few years have large-scale periodic structures been fabricated at a sufficiently small nanoscale [5] to operate in the visible spectral regime forming optical metamaterials [6,7].

In this paper, we move beyond linear properties to the nonlinearities of three-dimensional (3D) optical metamaterials. Their third-order nonlinear optical susceptibility is investigated using pump-probe spectroscopy, widely employed in examining metallic nanostructures with plasmonic resonances [8–13]. The intrinsic third-order nonlinear optical response of the metal and the effect on the plasmonic modes is, therefore, well understood. Furthermore, it has been shown that optically induced transient changes of the nanostructure optical properties can be enhanced by delocalizing the plasmonic modes which are trapped in subwavelength nanostructures when forming metamaterials [14].

Here we apply pump-probe techniques to a subwavelength, highly interconnected, 3D optical metamaterial. The nonlinear response is found to be 10–1000 times stronger than previously reported nanostructures [8–16], with complicated spectral signatures. This response is tuned by spectrally shifting the modified metamaterial plasma frequency when changing the background refractive index in which the nanostructure is embedded. An analytical model, relating the metamaterial effective dielectric function to the constituent gold, accounts for the main observations. This demonstrates how small optical perturbations in the gold within this composite nanostructure produce large modifications in the emergent optical properties of this highly interconnected metamaterial.

II. FABRICATION

Recent developments in self-assembly techniques [17] have made possible the fabrication of 3D metallic nanostructures, opening routes for the realization of 3D optical nanoplasmonic metamaterials [18,19]. So far, the only truly scalable such structure is the metallic single-gyroid metamaterial based on a triply periodic nanostructure composed of chiral bicontinuous networks derived from constant mean-curvature surfaces [20–22] [Fig. 1(a)]. We recently demonstrated that their optical properties can be easily

*jjb12@cam.ac.uk

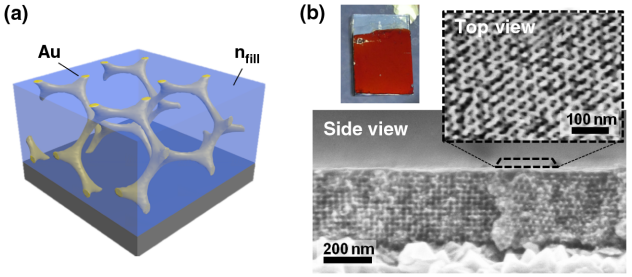

FIG. 1. (a) Gyroid nanostructure embedded in a dielectric with refractive index n_{fill}. (b) SEM images showing the cross-section through a gyroid, along with the top surface of the film (inset), and a photo of gyroid nanostructured film (top left).

tuned through the unit cell size ($a = 30$–50 nm $\ll \lambda$), fill fraction (f, tuned by strut thickness), and refractive index of the filling (n_{fill}) [23].

Our films are fabricated by casting the self-assembled morphology of a block copolymer in the gyroidal phase into Au [20,23]. Briefly, a polyisoprene-block-polystyrene-block-polyethylene oxide terpolymer assembles into two interpenetrating, chemically distinct gyroid networks (isoprene and ethylene oxide) embedded in a majority phase (styrene). The polyisoprene network is selectively degraded by UV radiation and removed before refilling via Au electrodeposition to provide thick films with a uniform top surface [Fig. 1(b)]. Samples are prepared on fluorine-doped-tin-oxide coated glass substrates. Here, two identical gyroid geometries are compared with $a = 35$ nm and 30% Au fill fraction, differing only in the choice of refractive index for the fill medium. In one set, the polymer template remained ($n_{\text{fill}} = 1.6$), while for the other set it was removed ($n_{\text{fill}} = 1$). A bulk-gold reference film is also electrodeposited under identical conditions. These three samples sit on identical substrates and each has a film thickness of 330 nm (~10 unit cells), which is sufficiently thick to clearly observe the metamaterial properties of the gyroids and to avoid transmission through the control bulk-gold sample.

III. LINEAR OPTICAL RESPONSE

Such gyroidal metamaterials have a completely different optical response to bulk Au, with a strongly redshifted plasma edge and transmission 8 orders of magnitude larger than would be expected from a bulk film with the same volume of metal (100 nm thick). As first shown by Pendry *et al.* [24], the electromagnetically driven electrons in such sub-λ nanostructures induce magnetic fields opposing their motion, which govern the effective macroscopic optical behavior of the structure. It was recently shown [21,23,25] that gold gyroid films behave as an artificial chiral plasma, with a Drude-like effective electric permittivity given by (see Appendix A and [25,26])

$$\varepsilon_{\text{gyr}} \simeq \frac{l\sqrt{2}}{a}\left[1 - \left(\frac{4r_g}{\lambda_g}\right)^2 \left(\frac{\pi\sqrt{-\varepsilon_m}}{2\sqrt{2}n_{\text{fill}}} - 1\right)^2\right], \qquad (1)$$

where λ_g is the effective plasma frequency of the perfect metal gyroid (dependent only on its geometry) and $r_g \simeq 0.29a\sqrt{f} = 5.6$ nm is the thinnest radius of the gyroid struts which have a normalized helix length l (for all structural parameters see Appendix A). The dielectric constants for bulk Au are modified (ε_m) by their sculpting into 10 nm struts, which enhances their damping contribution by a factor of 4 (as measured by comparing the four-point dc gyroid resistivity of $\rho_{\text{gyr}} = 52\ \mu\Omega\,\text{cm}$ to bulk films). This arises from the polycrystalline structure of the struts (seen in electron microscopy) so that electrons are forced to flow through grain boundaries and collide with the strut walls [27]. This damped Drude model is combined with the known interband contributions of Au which are strong below 500 nm. The modified Drude model allows the effective gyroid dielectric functions [Fig. 2(a)] to be calculated, showing the "dilution" of the negative real part of the metal components' permittivity within this nanoarchitecture.

The optical properties of gyroids are dominated by extra resonances and appear deep red when unfilled [Fig. 1(b)] due to a strong dip in reflectivity [Fig. 2(b)] around 530 nm, which tunes to 670 nm when filled with polymer. This dip is a consequence of a reflection null when the gyroid index matches the air above it, $\text{Re}(\varepsilon_{\text{gyr}}) = 1$, only possible in the metamaterial. The effective dielectric permittivity of the composite material [Fig. 2(a)] has a plasma frequency which can be significantly shifted into the red. Under simple assumptions (Appendix B), this dip wavelength is given by

$$\frac{\lambda_{\text{dip}}^2}{\lambda_p^2} \simeq \varepsilon_\infty + \frac{8n_{\text{fill}}^2}{\pi^2}\left(1 + \frac{\eta\lambda_g}{4r_g}\right)^2, \qquad (2)$$

where in the modified Drude model for bulk Au $\lambda_p = 146$ nm, $\varepsilon_\infty = 7.0$, and $\eta^2 = 1 - a/l\sqrt{2}$. This simple formula encapsulates the tuning dependence on the metal

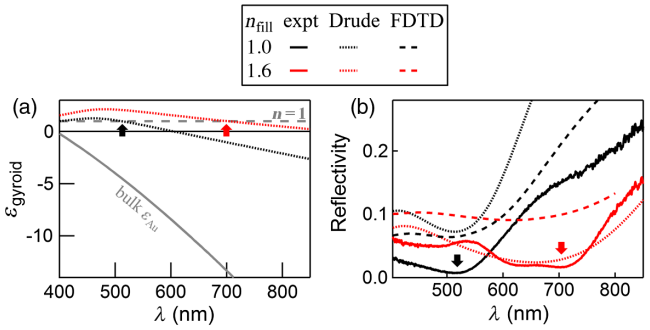

FIG. 2. (a) Effective dielectric functions of gyroids with refractive index filling $n_{\text{fill}} = 1$, 1.6 together with that of bulk Au (gray). (b) Reflectivity spectra for experimental gyroids (solid lines), analytic theory (dotted), and FDTD simulations (dashed), together with arrows showing spectral position of minimum reflectivity from the model (see text).

and its fill fraction, gyroid pitch, and dielectric filling. The positions of the wavelength dips are marked by arrows in Figs. 2(a) and 2(b) and match well the experimental data. The simulated reflectivity also provides a reasonable account of the measured spectra [Fig. 2(b)], with a good prediction of the dip wavelengths. Discrepancies arise from the approximations used above. The model ignores surface scattering (measured to be approximately 10%), which leads to a decrease in reflectivity. The double dip consistently seen in the measured reflectivity of the $n_{\text{fill}} = 1.6$ samples around 650 nm is not replicated in the simulations, but comes from weak thin-film interference arising in the transmissive gyroid films, not included in our model. A full finite-difference time-domain (FDTD) model is also used to confirm these analytic results (dashed), which also matches both experiment and the approximated analytic model.

IV. NONLINEAR OPTICAL RESPONSE

Our focus here is on the nonlinear optical properties of metallic nanostructures which are best characterized using ultrafast time-resolved techniques that can separate the different components of the response and reveal their dynamics. We use a narrow-band 200-fs λ-tunable pump pulse together with broadband probe pulses, allowing for the simultaneous measurement of pump-induced reflection changes across 490–750 nm. To achieve this, two synchronized Ti:sapphire regenerative amplifiers are both fed with the split output of a passively mode-locked Ti:sapphire oscillator, producing synchronized 800 nm beam lines of 200-fs pulses at a 250-kHz repetition rate. The tunable pump pulses are produced from an optical parametric amplifier in one beam line, while the second beam line is tightly focused into a 1.5-mm-thick sapphire crystal producing a supercontinuum used as the probe pulses [Fig. 3(a)]. The pump pulses are modulated at 1.6 kHz

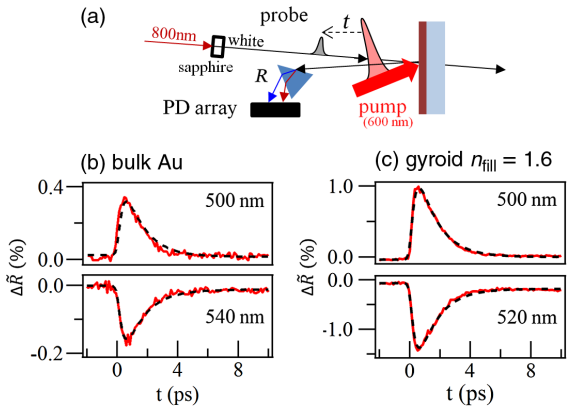

FIG. 3. (a) Schematic of pump-induced change in spectral reflection extracted from photodiode array. Transient reflectivity of (b) bulk gold and (c) gyroid sample with $n_{\text{fill}} = 1.6$ at selected probe wavelengths. The fits (dashed) allow extraction of the electronic, lattice, and thermal responses (see text).

and pump-induced changes to the probe reflectivity (ΔR) are measured using a 256-pixel custom-linear photodiode array with an electronic rolling shutter synchronized to the pump-modulation frequency [28]. A Brewster prism spectrally separates the supercontinuum across the array, simultaneously extracting $\Delta R(\lambda)$ in a single measurement with 1-nm resolution and a sensitivity of $\Delta R \simeq 10^{-4}$.

A pump wavelength of 600 nm is chosen to minimize direct excitation of interband transitions, while maintaining strong absorption in the gyroids. Average power densities up to 2 W/cm^2 could be used without laser-induced degradation of the intricate nanostructure, hence a pump power of 0.7 mW (3 nJ pulse energy) is focused onto a 250-μm-wide spot on the sample (1.4 W/cm^2), with a spectrally integrated probe power of 100 μW (0.4 nJ) confined to the inner 150 μm. To minimize pump scatter in the probe direction, the angles of incidence of pump and probe beams are 30° and 10°, respectively. In the gyroid films, the domain sizes are on the μm scale, so that polarization effects average out over the much larger probed area, and no strong polarization sensitivity is observed.

The pump-induced transient reflectivity of the gyroid films (normalized as $\Delta\tilde{R} = \Delta R/R$) is found to be an order of magnitude larger than that of bulk gold and exhibits a rather different spectral dependence [Fig. 3(b)]. In spite of the nanostructured architecture, all relaxation times remained unaffected, suggesting that the conventional two-temperature model can be used for interpreting the microscopic Au response [29,30]. In this scheme, the electronic and lattice temperatures of the metal decouple, allowing them to be separated. Two relaxation mechanisms are considered, the electron-electron scattering rate α and the electron-phonon scattering rate β, which is typically slower by a factor of 4. The response

$$\Delta\tilde{R}(t) = [\Delta\tilde{R}_e(1 - e^{-t\alpha})e^{-t\beta} + \Delta\tilde{R}_\ell(1 - e^{-t\beta})]_{t>0} + \Delta\tilde{R}_t \tag{3}$$

tracks the electronic response (e) which increases as electron-electron scattering redistributes the energy from photoexcited electrons to the rest of the electron body. These hot electrons subsequently equilibrate with the lattice (ℓ) through electron-phonon scattering. The locally heated lattice equilibrates through heat diffusion on a time scale which is much longer than considered here, producing a thermal offset (t) from residual heating by the previous pulse. This function fits the measured signals [dashed lines in Fig. 3(b)] when convolved with a pulse width of 200 fs, for $\alpha = 2.7$ ps^{-1} and $\beta = 0.75$ ps^{-1} matching values reported for bulk Au [31,32]. While it might be expected that a modified phonon density of states from the strut confinement can alter β, little change is seen. This is likely due to the dominance of high-energy electrons in the lattice coupling beyond any low-q cutoff from the narrow strut.

We now concentrate on the spectral dependence of the dominant initial electronic response, which is a direct result of the increase in electron temperature from the energy deposited by the optical pulse. The most important change to the metal's optical properties from an elevated electron temperature is an increase of the electron damping rate, Γ [33,34]. In addition to this, there are also modifications to the interband transitions below 500 nm from changes in electron occupation near the Fermi level, which have been successfully modeled [35] using relativistic band-structure calculations [36]. The measured pump-induced reflectivity change of the bulk-gold film is well reproduced by increasing damping in the Drude model for Au by $\Delta\Gamma =$ 3 meV (with additional short wavelength changes due to induced changes in the interband transitions). For wavelengths longer than these interband transitions, the induced reflectivity is always negative. This gives a good account of the typical Au nonlinear response [dashed line in Fig. 4(a)]. This model would suggest that the nonlinear response should be proportional to pump power, which is indeed observed at all wavelengths.

In plasmonic materials, the resonant plasmon peak is typically transiently broadened by this perturbation. On the other hand, in interconnected metamaterials the response arises from a different coupling to the composite dielectric function. The gyroid transient-reflectivity spectra from the pump-induced electronic changes to the Au struts shows a much more complicated and stronger spectral response [Fig. 4(b)]. We find induced changes which can exceed 5%, more than one order of magnitude larger than the best plasmonic materials or bulk Au. Similar results are seen in 600-nm-thick gyroid films, and the reflectivity changes are found to scale linearly with incident pump power. A consistent positive response is seen from the polymer-filled gyroid at wavelengths shorter than its near-infrared effective plasma wavelength. Figure 4(b) shows that the sign of the nonlinear reflectivity is inverted by filling an electronically passive dielectric component into the gyroid network. Such a manipulation of the nonlinear susceptibility is one of the features of metamaterials.

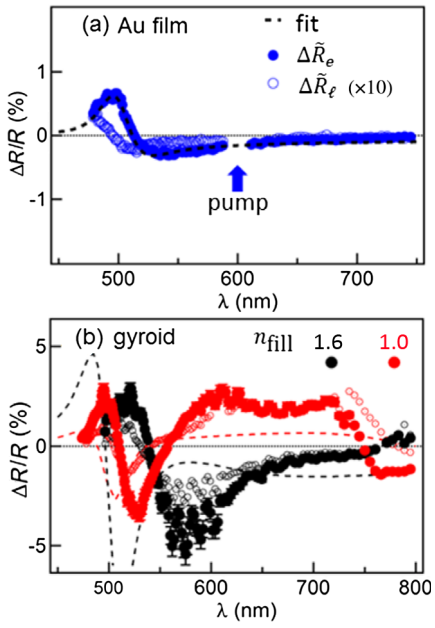

FIG. 4. Magnitude of extracted electronic (•) and lattice (◦) components of the transient reflectivity $\Delta\tilde{R}_{e,\ell}$ as a function of probe wavelength for (a) solid-gold films and (b) two gyroid samples of different n_{fill}. FDTD fits are shown dashed and magnified ×5 in (b).

Modeling the full metamaterial nonlinear response is more complex, as both geometric and material responses are coupled. We utilize FDTD simulations [dashed lines in Figs. 4(a) and 4(b)] that assume the dielectric function of the gold forming the gyroidal structure is modified in the same manner as the bulk-gold sample, successfully predicting the sign of the long-wavelength response. The strong enhancement in magnitude observed in gyroids can be partially attributed to the increased ability of the struts of gold to absorb light compared to bulk Au, due to the enhanced surface fields which propagate along the struts. Further enhancement arises from the greater sensitivity of the gyroid response to the dielectric properties of its metallic components. While some of the observed spectral features have different magnitudes, the key finding of an opposite sign of response when changing the refractive index of the gyroid matrix is matched. Similar results are obtained by using the analytical model, with the inversion of $\Delta\tilde{R}$ produced when increasing the Drude damping or the background permittivity, however, the presence of the interband contributions means that no unambiguous fit is robust. An improved theory of such metamaterials is thus required in order to understand the full details of the nonlinear spectral response.

The lattice contributions at long time scales [Fig. 4(b), ◦] follow a similar spectral response to the electronic changes, although they are one order of magnitude smaller. This confirms that excitation-induced modification to the distribution of electrons within the metal is filtered by the gyroid geometrical electromagnetic response to give the observed nonlinear enhanced reflection signature. The observed transient spectral changes are little affected by the exact pump wavelength (just as for bulk Au) because the heating of electrons depends only on absorbed energy. The magnitude of the nonlinear response thus follows the gyroid absorption. This is greatly enhanced over bulk-Au absorption because of the way light enters the structure and is enhanced close to the Au struts. Of great interest would be the exploration of pump-induced changes in the gyroid chiral response, which was previously demonstrated in Ref. [20], however, this requires propagation along specific directions at high angles to the film surface, and large enough single domains for pump-probe spectroscopies, which is not yet feasible. Such measurements would reveal the ability to switch on and off negative refraction at ultrafast speeds.

V. SUMMARY

In conclusion, 3D gyroid metamaterials with a tunable plasma frequency show dramatically enhanced changes in reflectivity and absorption on injecting short pulses of light. We extract the electronic and lattice contribution to the nonlinear response, and show how these change when tuning the metamaterial through gyroid filling. Both FDTD simulations and a simple analytical model can account for the main features of the complex spectral response. The sign of these nonlinear changes can be explained from shifts in the spectral position at which the metamaterial index matches to air. The remarkable strength of the nonlinearity can be attributed to a genuine metamaterial effect: because of the collective nanoplasmonic metamaterial network, the effective linear permittivity and linear refractive index are dramatically reduced (Fig. 2) and thus the next-highest-order contribution which is the nonlinear response becomes more and more dominant. The fill fraction of the interconnected nanostructures which confine the light is very high, and withstands the parasitic coupling that normally reduces the response when plasmonic structures are densely packed. These tunable third-order nonlinear responses can thus be enhanced and easily tuned inside metamaterials, opening the way to new sensing modalities as well as nonlinear and active devices [37,38].

ACKNOWLEDGMENTS

We acknowledge EPSRC Grants No. EP/G060649/1, No. EP/G037221/1, No. EP/L015978/1, No. EP/L027151/1, NanoDTC, and ERC Grant LINASS (No. 320503). U. W. thanks the National Science Foundation for support through a Materials World Network grant between the U.S. (No. DMR-1008125) and the U.K. EPSRC.

APPENDIX A: THE EFFECTIVE PERMITTIVITY OF GYROIDAL METAMATERIALS

We first develop an analytic approximate formula for the effective dielectric constant of the gyroid and use this formula to estimate the position of the dip in the reflection spectrum. We have previously derived the electromagnetic properties of the gyroid [21,25], where we found that the effective chirality and magnetic (H) permittivity are negligible compared to the electric (E) permittivity. Since chirality is several orders of magnitude smaller than the electric permittivity (i.e., $\chi_{EH} = \chi_{HE} \to 0$), the derived electric permittivity of the gyroid [25] can be reduced to

$$\varepsilon_{\mathrm{gyr}} = \chi_{EE} = \frac{\chi_{HH}^{-1}}{\varepsilon_{0\mu_0}[c_0^2\chi_{EE}^{-1}\chi_{HH}^{-1} + \varepsilon_0\mu_0(\chi_{EH}^{-1})^2]} = \frac{l}{b}\left[1 - \frac{\omega_g^2}{(\omega')^2 + i\Gamma\omega'}\right] + I(f, \varepsilon_{\mathrm{ib}}, n_{\mathrm{fill}}). \quad \text{(A1)}$$

Here l is the length of the helical wires forming the gyroid (defined below), $b = a/\sqrt{2}$ for a unit cell size a, and ω_g is the effective plasma frequency for a perfect metal gyroid which depends also on the geometry of the nanostructure (defined below). The final term $I(f, \varepsilon_{\mathrm{ib}}, n_{\mathrm{fill}})$ is appended to account for the near-infrared interband transitions using a single Lorentzian ($\varepsilon_{\mathrm{ib}}$), which is scaled by a Maxwell-Garnett approximation to account for the metal filling fraction (f) in the gyroid films and the refractive index of the embedding material (n_{fill}).

Since metals at optical frequencies have relatively high resistivity and are completely penetrated by the incident electromagnetic field, we need to correct the above derivation (which was performed assuming good conductors) to account for the delayed electron flow [26]. Following our work in Ref. [26], we can model the flow of electrons in optical metallic structures as waves propagating in a waveguide, and therefore we account for the slower electron movement by replacing ω' in Eq. (A1) with

$$\omega' = \frac{\omega}{\kappa - \frac{2r_g\omega}{\pi c_0}}, \quad \text{(A2)}$$

where c_0 is the speed of light and κ is a function depending only on the permittivity of the metal forming the optical metallic structure, defined as

$$\kappa^{-1} = n_{\mathrm{fill}}\sqrt{1 - \frac{2}{\varepsilon_m}\left(\frac{\lambda}{2\pi r_g z_4}\right)^2}, \quad \text{(A3)}$$

where $\varepsilon_{\mathrm{fill}}$ is the permittivity of the medium surrounding the gyroid metal struts and r_g is the radius of the metal struts (defined below).

Here, z_4 is a function of the metal's electric permittivity [26] and the medium around the metal ($\varepsilon_{\mathrm{fill}}$), which are the dominant influence on the electron flow in the metal at optical wavelengths. However, for all the cases considered here $z_4 \simeq 1$ (Fig. 5) and can therefore be neglected.

The dielectric permittivity of Au in the gyroids, ε_m, is not exactly the same as that of bulk Au, due to the polycrystalline nature of the struts and the way current is forced to travel through grain boundaries. Because the strut radius is

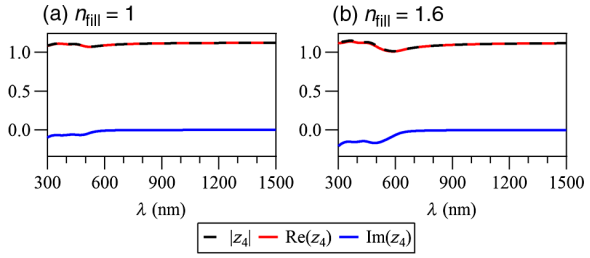

FIG. 5. Spectral function z_4 plotted for (a) $n_{\mathrm{fill}} = 1$ and (b) $n_{\mathrm{fill}} = 1.6$, for Au.

much smaller than the visible wavelengths considered here, the expression for κ is accurately given by

$$\kappa^{-1} \simeq \frac{\lambda n_{\text{fill}}}{2\pi r_g}\sqrt{\frac{2}{-\varepsilon_m}}. \tag{A4}$$

If we assume that all losses in the electric permittivity of the gyroid are due to the metal losses, $\Gamma \to 0$ in Eq. (A1), leading to

$$\varepsilon_{\text{gyr}} = \frac{l}{b}\left[1 - \frac{\omega_g^2}{\omega^2}\left(\kappa - \frac{2r_g\omega}{\pi c_0}\right)^2\right], \tag{A5}$$

$$\varepsilon_{\text{gyr}} \simeq \frac{l}{b}\left[1 - \left(\frac{4r_g}{\lambda_g}\right)^2\left(\frac{\pi\sqrt{-\varepsilon_m}}{2\sqrt{2}n_{\text{fill}}} - 1\right)^2\right]. \tag{A6}$$

The geometrical parameters of the gyroid are defined as

$$\begin{aligned} b &= \frac{a}{\sqrt{2}}, \\ R &= \frac{2-\sqrt{2}}{4}b = \frac{\sqrt{2}-1}{4}a \simeq 1.193a, \\ l &= \sqrt{(2\pi R)^2 + a^2} = a\sqrt{\frac{\pi^2(\sqrt{2}-1)^2}{4} + 1}, \\ r_g &= a\sqrt{f}\,\frac{\sqrt[4]{2}}{\sqrt{\pi[\sqrt{2+\pi^2} + \sqrt{2+(3+2\sqrt{2})\pi^2}]}}, \\ &\simeq 0.29a\sqrt{f}, \end{aligned} \tag{A7}$$

and the effective plasma frequency of the perfect gyroid derived in Ref. [25] is

$$\lambda_g = \frac{2\pi R b}{a}\sqrt{\pi\left(1 - \frac{\pi R^2}{a^2} + L\frac{a}{2\pi R}\right)}, \tag{A8}$$

where L is the self-inductance of the conductive parts of the gyroid given by $L = (l/b)\ln(\sqrt{b^3/\pi r^2 l})$. Simplifying this expression gives

$$\lambda_g = 1.15a\sqrt{1 - 0.65\ln f}, \tag{A9}$$

which is a weak function of the filling fraction f, and $\lambda_g = 1.54\ a = 54$ nm for the 30% filling fraction used here.

The effective dielectric constant of the gyroid is then given by

$$\varepsilon_{\text{gyr}} \simeq 1.69\left[1 - 1.35f\left(\frac{a}{\lambda_g}\right)^2\left(\frac{\sqrt{-\varepsilon_m}}{0.90n_{\text{fill}}} - 1\right)^2\right], \tag{A10}$$

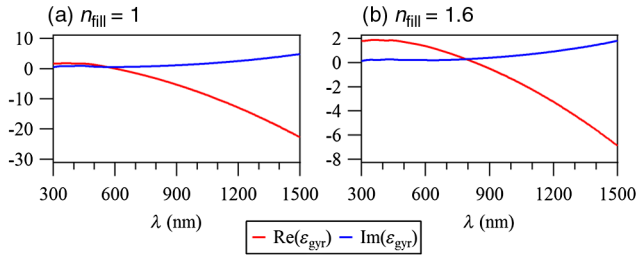

FIG. 6. Effective gyroid dielectric function ε_{gyr} plotted for (a) $n_{\text{fill}} = 1$ and (b) $n_{\text{fill}} = 1.6$, for Au.

which is used in the main text. This approximate expression for the dielectric constant scales with the refractive index of the material filling the gyroid, the metal forming the gyroids, and the metal filling fraction. We note that ε_{gyr} does *not* change with the unit cell size, which might indeed be expected for a metamaterial with feature sizes much smaller than the optical wavelength. The effective dielectric permittivity of the gyroid is plotted in Fig. 2(a) in the main text. This can be compared with the exact complex permittivity from the full model above (Fig. 6).

APPENDIX B: DERIVATION OF λ_{dip}

To estimate the spectral position of the dip in reflection, we assume that it occurs when the optical properties of the gyroid are matched with air. This is reached when the electric permittivity of the gyroid sample (ε_{gyr}) is approximately equal to the permittivity of air (ε_{air}):

$$\varepsilon_{\text{gyr}} = \varepsilon_{\text{air}} = 1. \tag{B1}$$

Rearranging the expression for ε_{gyr}, we find this condition occurs when

$$\sqrt{-\varepsilon_m} \simeq \left(1 + \frac{\eta\lambda_g}{4r_g}\right)\frac{2\sqrt{2}}{\pi}n_{\text{fill}}, \tag{B2}$$

where $\eta = \sqrt{1 - b/l} = 0.64$.

We can solve this expression using the tabulated permittivity for Au modified by the increased damping discussed above, or we can adopt a Drude model

$$\varepsilon_m = \varepsilon_\infty - \frac{\omega_p^2}{\omega^2 + i\Gamma_p\omega}, \tag{B3}$$

where the optimal values for the Drude coefficients in the visible and near-infrared region are given here by $\omega_p = 2\pi c_0/\lambda_p = 9.05$ eV and $\Gamma_p = 0.3$ eV. Substituting this expression allows us to solve for the reflection minimum,

$$\lambda_{\text{dip}}^{-2} \simeq \lambda_p^{-2}\left\{\varepsilon_\infty + \left[n_{\text{fill}}\frac{2\sqrt{2}}{\pi}\left(1 + \frac{\eta\lambda_g}{4r_g}\right)\right]^2\right\}^{-1} - \left(\frac{\Gamma_p}{2\pi c_0}\right)^2. \tag{B4}$$

Ignoring the small contribution that comes from the damping term (which only shifts the spectral positions of the reflectivity minimum by ∼10 nm), gives the equation in the main text.

[1] Y. Liu and X. Zhang, Metamaterials: A new frontier of science and technology, Chem. Soc. Rev. **40**, 2494 (2011).

[2] Z. Li, M. Mutlu, and E. Ozbay, Chiral metamaterials: From optical activity and negative refractive index to asymmetric transmission, J. Opt. **15**, 023001 (2013).

[3] R. A. Shelby, D. R. Smith, and S. Schultz, Experimental verification of a negative index of refraction, Science **292**, 77 (2001).

[4] J. B. Pendry, Negative refraction makes a perfect lens, Phys. Rev. Lett. **85**, 3966 (2000).

[5] V. K. Valev, B. De Clercq, C. G. Biris, X. Zheng, S. Vandendriessche, M. Hojeij, D. Denkova, Y. Jeyaram, N. C. Panoiu, Y. Ekinci, A. V. Silhanek, V. Volskiy, G. A. E. Vandenbosch, M. Ameloot, V. V. Moshchalkov, and T. Verbiest, Distributing the optical near-field for efficient field-enhancements in nanostructures, Adv. Mater. **24**, OP208 (2012).

[6] J. Valentine, S. Zhang, T. Zentgraf, E. Ulin-Avila, D. A. Genov, G. Bartal, and X. Zhang, Three-dimensional optical metamaterial with a negative refractive index, Nature (London) **455**, 376 (2008).

[7] M. D. Turner, M. Saba, Q. Zhang, B. P. Cumming, G. E. Schröder-Turk, and M. Gu, Miniature chiral beamsplitter based on gyroid photonic crystals, Nat. Photonics **7**, 801 (2013).

[8] G. Della Valle, F. Scotognella, A. R. S. Kandada, M. Zavelani-Rossi, H. Li, M. Conforti, S. Longhi, L. Manna, G. Lanzani, and F. Tassone, Ultrafast optical mapping of nonlinear plasmon dynamics in $Cu_{2-x}Se$ nanoparticles, J. Phys. Chem. Lett. **4**, 3337 (2013).

[9] R. D. Averitt, S. L. Westcott, and N. J. Halas, Ultrafast electron dynamics in gold nanoshells, Phys. Rev. B **58**, R10203 (1998).

[10] J.-Y. Bigot, J.-Y. Merle, O. Cregut, and A. Daunois, Electron dynamics in copper metallic nanoparticles probed with femtosecond optical pulses, Phys. Rev. Lett. **75**, 4702 (1995).

[11] C. Voisin, N. Del Fatti, D. Christofilos, and F. Vallee, Ultrafast electron dynamics and optical nonlinearities in metal nanoparticles, J. Phys. Chem. B **105**, 2264 (2001).

[12] A. Kubo, K. Onda, H. Petek, Z. Sun, Y. S. Jung, and H. K. Kim, Femtosecond imaging of surface plasmon dynamics in a nanostructured silver film, Nano Lett. **5**, 1123 (2005).

[13] M. Ren, E. Plum, J. Xu, and N. I. Zheludev, Giant nonlinear optical activity in a plasmonic metamaterial, Nat. Commun. **3**, 833 (2012).

[14] G. A. Wurtz, R. Pollard, W. Hendren, G. P. Wiederrecht, D. J. Gosztola, V. A. Podolskiy, and A. V. Zayats, Designed ultrafast optical nonlinearity in a plasmonic nanorod metamaterial enhanced by nonlocality, Nat. Nanotechnol. **6**, 107 (2011).

[15] D. J. Cho, W. Wu, W. Ponizovskaya, P. Chaturvedi, A. M. Bratkovsky, S.-Y. Wang, X. Zhang, F. Wang, and Y. R. Shen, Ultrafast modulation of optical metamaterials, Opt. Express **17**, 17652 (2009).

[16] K. Appavoo, B. Wang, N. F. Brady, M. Seo, J. Nag, R. P. Prasankumar, D. J. Hilton, S. T. Pantelides, and R. F. Haglund Jr., Ultrafast phase transition via catastrophic phonon collapse driven by plasmonic hot-electron injection, Nano Lett. **14**, 1127 (2014).

[17] D. A. Pawlak, S. Turczynski, M. Gajc, K. Kolodziejak, R. Diduszko, K. Rozniatowski, J. Smalc, and I. Vendik, How far are we from making metamaterials by self-organization? The microstructure of highly anisotropic particles with an srr-like geometry, Adv. Funct. Mater. **20**, 1116 (2010).

[18] A. C. Edrington, A. M. Urbas, P. DeRege, C. X. Chen, T. M. Swager, N. Hadjichristidis, M. Xenidou, L. J. Fetters, J. D. Joannopoulos, and Y. Fink, Polymer-based photonic crystals, Adv. Mater. **13**, 421 (2001).

[19] I. Vukovic, S. Punzhin, Z. Vukovic, P. Onck, J. T. M. De Hosson, G. ten Brinke, and K. Loos, Supramolecular route to well-ordered metal nanofoams, ACS Nano **5**, 6339 (2011).

[20] S. Vignolini, N. A. Yufa, P. S. Cunha, S. Guldin, I. Rushkin, M. Stefik, K. Hur, U. Wiesner, J. J. Baumberg, and U. Steiner, A 3D optical metamaterial made by self-assembly, Adv. Mater. **24**, OP23 (2012).

[21] S. S. Oh, A. Demetriadou, S. Wuestner, and O. Hess, On the origin of chirality in nanoplasmonic gyroid metamaterials, Adv. Mater. **25**, 612 (2013).

[22] K. Hur, Y. Francescato, V. Giannini, S. A. Maier, R. G. Hennig, and U. Wiesner, Three-dimensionally isotropic negative refractive index materials from block copolymer self-assembled chiral gyroid networks, Angew. Chem. **123**, 12191 (2011).

[23] S. Salvatore, A. Demetriadou, S. Vignolini, S. S. Oh, S. Wuestner, N. A. Yufa, M. Stefik, U. Wiesner, J. J. Baumberg, O. Hess, and U. Steiner, Tunable 3D extended self-assembled gold metamaterials with enhanced light transmission, Adv. Mater. **25**, 2713 (2013).

[24] J. B. Pendry, A. J. Holden, W. J. Stewart, and I. Youngs, Extremely low frequency plasmons in metallic mesostructures, Phys. Rev. Lett. **76**, 4773 (1996).

[25] A. Demetriadou, S. S. Oh, S. Wuestner, and O. Hess, A tri-helical model for nanoplasmonic gyroid metamaterials, New J. Phys. **14**, 083032 (2012).

[26] A. Demetriadou and O. Hess, Analytic theory of optical nanoplasmonic metamaterials, Phys. Rev. B **87**, 161101 (2013).

[27] C. Durkan and M. E. Welland, Size effects in the electrical resistivity of polycrystalline nanowires, Phys. Rev. B **61**, 14215 (2000).

[28] R. J. Smith, R. A. Light, S. D. Sharples, N. S. Johnston, M. C. Pitter, and M. G. Somekh, Multichannel, time-resolved picosecond laser ultrasound imaging and spectroscopy with custom complementary metal-oxide-semiconductor detector, Rev. Sci. Instrum. **81**, 024901 (2010).

[29] G. L. Eesley, Phys. Rev. B **33**, 2144 (1986).

[30] R. W. Schoenlein, W. Z. Lin, J. G. Fujimoto, and G. L. Eesley, Femtosecond studies of nonequilibrium electronic processes in metals, Phys. Rev. Lett. **58**, 1680 (1987).

[31] W. S. Fann, R. Storz, H. W. K. Tom, and J. Bokor, Direct measurement of nonequilibrium electron-energy

distributions in subpicosecond laser-heated gold films, Phys. Rev. Lett. **68**, 2834 (1992).

[32] P. Farah, N. Gibbons, F. M. Huang, and J. J. Baumberg, Ultrafast nonlinearities of minibands in metallodielectric Bragg resonators, Phys. Rev. B **84**, 125442 (2011).

[33] D. T. Owens, C. Fuentes-Hernandez, J. M. Hales, J. W. Perry, and B. Kippelen, A comprehensive analysis of the contributions to the nonlinear optical properties of thin Ag films, J. Appl. Phys. **107**, 123114 (2010).

[34] A. Alabastri, S. Tuccio, A. Giugni, A. Toma, C. Liberale, G. Das, D. DeAngelis, E. DiFabrizio, and R. P. Zaccaria, Molding of plasmonic resonances in metallic nanostructures: Dependence of the non-linear electric permittivity on system size and temperature, Materials **6**, 4879 (2013).

[35] R. Rosei, F. Antonangeli, and U. Grassano, d bands position and width in gold from very low temperature thermomodulation measurements, Surf. Sci. **37**, 689 (1973).

[36] N. Christensen and B. Seraphin, Relativistic band calculation and the optical properties of gold, Phys. Rev. B **4**, 3321 (1971).

[37] O. Hess, J. B. Pendry, S. A. Maier, R. F. Oulton, J. M. Hamm, and K. L. Tsakmakidis, Active nanoplasmonic metamaterials, Nat. Mater. **11**, 573 (2012).

[38] A. D. Neira, G. A. Wurtz, P. Ginzburg, and A. V. Zayats, Opt. Express **22**, 10987 (2014).